Earth's Future

RESEARCH ARTICLE
10.1029/2024EF005011

IMO2020 Regulations Accelerate Global Warming by up to 3 Years in UKESM1

G. Jordan[1] and M. Henry[2]

[1]Met Office Hadley Centre, Exeter, UK, [2]Department of Mathematics, University of Exeter, Exeter, UK

Key Points:

- Recent regulations on the sulfur content of ship emissions has accelerated global warming by approximately 2–3 years
- Reduced ship emissions induce responses in cloud properties, top-of-atmosphere radiation, and surface temperatures
- The regulations contribute to the exceptional warming observed in 2023, yet other factors are needed to fully account for it

Supporting Information:

Supporting Information may be found in the online version of this article.

Correspondence to:

G. Jordan,
george.jordan@metoffice.gov.uk

Citation:

Jordan, G., & Henry, M. (2024). IMO2020 regulations accelerate global warming by up to 3 years in UKESM1. *Earth's Future*, *12*, e2024EF005011. https://doi.org/10.1029/2024EF005011

Received 12 JUN 2024
Accepted 3 AUG 2024

Abstract The International Maritime Organization (IMO) introduced new regulations on the sulfur content of shipping emissions in 2020 (IMO2020). Estimates of the climatic impact of this global reduction in anthropogenic sulfate aerosols vary widely. Here, we contribute to narrowing this uncertainty with two sets of climate model simulations using UKESM1. Using fixed sea-surface temperature atmosphere-only simulations, we estimate an IMO2020 global effective radiative forcing of 0.139 ± 0.019 Wm^{-2} and show that most of this forcing is due to aerosol-induced changes to cloud properties. Using coupled ocean-atmosphere simulations, we note significant changes in cloud top droplet number concentration and size across regions with high shipping traffic density, and—in the North Atlantic and North Pacific—these microphysical changes translate to a decrease in cloud albedo. We show that IMO2020 increases global annual surface temperature on average by 0.046 ± 0.010°C across 2020–2029; approximately 2–3 years of global warming. Furthermore, our model simulations show that IMO2020 helps to explain the exceptional warming in 2023, but other factors are needed to fully account for it. The year 2023 also had an exceptionally large decrease in reflected shortwave radiation at the top-of-atmosphere. Our results show that IMO2020 made that more likely, yet the observations are within the variability of simulations without the reduction in shipping emissions. To better understand the climatic impacts of IMO2020, a model intercomparison project would be valuable whilst the community waits for a more complete observational record.

Plain Language Summary In 2020, the International Maritime Organization introduced new regulations decreasing the sulfur content of shipping emissions (IMO2020). Since sulfur is a pollutant, it is expected that IMO2020 will improve air quality and health outcomes. These emissions, however, also lead to the formation of tiny particles in the air which brighten clouds, resulting in more sunlight reflected to space which helps cool the planet. Hence, by reducing sulfur emissions, IMO2020 will lead to planetary warming, yet the magnitude of this effect is hotly debated. In this work, we use a state-of-the-art Earth system model to assess the warming impact of IMO2020. We find that IMO2020 increases the global average temperature by around 0.05°C; the equivalent to 2–3 years of global warming. Thus, IMO2020 helps to explain the exceptional warmth observed in 2023, yet other factors are needed to fully account for it. The year 2023 also had a record decrease in reflected sunlight contributing to the record temperatures, and our results show that IMO2020 made that more likely. Finally, we emphasize that IMO2020 has simply brought forward the warming from reductions in pollutants that are factored in favorable future climate scenarios.

1. Introduction

For decades, emissions from international shipping have released many pollutants, including sulfur dioxide (SO_2), which—once oxidized—forms sulfate aerosol (SO_4^{2-}) in the atmosphere (Eyring et al., 2010). With around 13% of global anthropogenic SO_2 emissions released along the world's shipping lanes (Faber et al., 2021; Smith et al., 2015), the detrimental effects relating to air quality (e.g., Contini & Merico, 2021; Mueller et al., 2023) and ocean acidification (e.g., Hassellöv et al., 2013; Jägerbrand et al., 2019) are experienced globally. Mitigating these adverse impacts falls under the remit of the International Maritime Organization (IMO). A recent IMO regulation—"IMO2020"—lowered the global maximum limit on the sulfur mass content in ship exhaust gases from 3.5% to 0.5% (IMO, 2019). Enforced on 1 January 2020, IMO2020 has ushered in shipping's low-sulfur era prompting fuel and structural changes to vessels and their operations (e.g., Chu Van et al., 2019; Kuittinen et al., 2021; Solakivi et al., 2019) that is estimated to have reduced annual shipping SO_2 emissions by 8.5 Mt of SO_2 (Sofiev et al., 2018); approximately 10% of annual global anthropogenic SO_2 emissions in 2019 (Forster et al., 2024; O'Rourke et al., 2021). Studies have projected that IMO2020 will result in improvements in air quality, and decreases in mortality and morbidity

rates (Partanen et al., 2013; Sofiev et al., 2018). However, shifting to low-sulfur fuel and reducing atmospheric SO_4^{2-} concentrations also has climatic consequences due to the influence of aerosols on the Earth's energy imbalance (e.g., Bellouin et al., 2020, and others).

Aerosols affect the Earth's energy budget via direct and indirect mechanisms. The former corresponds to the scattering and absorption of solar and terrestrial radiation by the aerosol itself (e.g., Myhre et al., 2013, and others), whereas the latter involves the modification of cloud properties via the role of aerosols as cloud condensation nuclei (CCN). For liquid clouds, as aerosol concentration increases, so does the number of CCN which increases the cloud droplet number concentration (N_d) (Twomey, 1974). If the liquid water content of a cloud remains constant, the increased N_d reduces the cloud droplet size (the effective radius, r_e) increasing cloud albedo (A_{cld}), thus inducing a cooling (Twomey, 1977). This chain of events is widely termed "the first indirect effect" or "Twomey effect." With smaller cloud droplets, the efficiency of collision-coalescence processes decreases which suppresses precipitation. Hence, aerosol-influenced clouds may have longer lifetimes and/or greater coverage (Albrecht, 1989), as well as increased cloud depth (Pincus & Baker, 1994), all of which further enhance A_{cld}, ergo the aerosol-induced cooling. These subsequent adjustments are collectively known as "the second indirect effect." Further cloud adjustments to the aerosol perturbation are thought to arise from entrainment processes and can act to reduce the magnitude of cooling (e.g., Ackerman et al., 2004; Bretherton et al., 2007; Small et al., 2009). Collectively, all these cloud modification processes are referred to as aerosol-cloud interactions (ACIs), and, due to the gradual reduction in anthropogenic aerosol emissions in recent decades, ACI cooling has diminished (Hodnebrog et al., 2024; Quaas et al., 2022). It is unsurprising then that IMO2020—a sharp reduction in aerosol—is often mentioned in discussions of a recent acceleration in the rate of warming, particularly in connection with the record breaking surface temperatures of 2023 (Hansen et al., 2023; Schmidt, 2024).

IMO2020 has had observable impacts on ship tracks. Watson-Parris et al. (2022) and Yuan et al. (2022) use independent machine-learning models to show that the transition to low-sulfur fuel has substantially reduced visible ship tracks. Moreover, Diamond (2023) analyses observed changes in cloud properties within a southeastern Atlantic Ocean shipping corridor following IMO2020, noting decreases in r_e and A_{cld}, and estimates an instantaneous radiative forcing (IRF) of $\mathcal{O}(1\ \mathrm{Wm}^{-2})$ within the study area which, when extrapolated globally, is $\mathcal{O}(0.1\ \mathrm{Wm}^{-2})$. This global observational estimate agrees with previous modeling studies that evaluate the radiative forcing of IMO2020 by comparing simulations of a globally enforced 0.5% sulfur limit with control simulations (Lauer et al., 2009; Partanen et al., 2013; Sofiev et al., 2018; Yuan et al., 2023). However, these studies all use models nudged using meteorological re-analysis data with fixed sea-surface temperatures (SSTs) and sea ice. Subsequently, the IMO2020 temperature response can only be estimated using simple climate models tuned to emulate historical behavior. To provide a more robust quantitative analysis, it is necessary to employ coupled atmosphere-ocean climate models which are able to resolve climate feedbacks interactively, as was done in (Quaglia & Visioni, 2024; Yoshioka et al., 2024). A summary of the forcing estimates of SO_2 emissions from shipping is given in Table A1, though caution should be used when comparing these values as they use different assumptions and experimental designs.

Our work aims to further our understanding on the climatic impact of IMO2020 by using both fixed SST atmosphere-only and coupled atmosphere-ocean simulations from the state-of-the-art Earth system model, UKESM1. Section 2 provides an overview of UKESM1 and a description of the experimental design. Section 3 presents the fixed SST atmosphere-only simulations, providing estimates of the IMO2020 radiative forcing, along with quantifying the contributions from the aerosol direct and indirect mechanisms. Section 4 shows the coupled atmosphere-ocean experiment results where we evaluate the IMO2020 influence on cloud micro- and macrophysical properties, along with assessing the surface temperature and top-of-atmosphere (ToA) radiation responses and how they relate to the observed record 2023 temperature anomalies. Finally, we summarize our results and conclude in Section 5.

2. Methodology

Here we provide a brief description of the ACI relevant components of UKESM1 and our experimental design, including our modeled estimate of the reduction on SO_2 shipping emissions caused by IMO2020.

2.1. UKESM1

UKESM1 (Sellar et al., 2019) uses the global coupled climate model HadGEM3-GC3.1 (Kuhlbrodt et al., 2018; Williams et al., 2018) as its physical core with the coupling of additional Earth system components including: atmospheric composition from the stratosphere-troposphere version of the UK Chemistry and Aerosol (UKCA) model (Archibald et al., 2020), ocean biogeochemistry from the Model of Ecosystem Dynamics, nutrient Utilisation, Sequestration and Acidification (MEDUSA, Yool et al., 2013), and terrestrial biogeochemistry from the Joint UK Land Environment Simulator (JULES, Best et al., 2011). UKESM1 treats aerosol number concentrations prognostically using the two-moment Global Model of Aerosol Processes (GLOMAP) modal aerosol microphysics scheme (Mann et al., 2010, 2012) for all aerosol species except for dust which uses the CLASSIC dust scheme (Woodward, 2001). For large-scale clouds (i.e., not convective), the activation of aerosols to cloud droplets is governed by the UKCA-Activate scheme (West et al., 2014) which incorporates the parameterization of Abdul-Razzak and Ghan (2000). Large-scale cloud precipitation formation is based on the one-moment scheme of Wilson and Ballard (1999) with autoconversion and accretion following the parameterization of Khairoutdinov and Kogan (2000). Large-scale cloud fraction, and cloud water vapor and liquid content are treated prognostically by the PC2 scheme (Wilson et al., 2008) with updates from Morcrette (2012). Convective cloud parameterizations are separate and do not account for aerosol or N_d meaning a convective component of aerosol forcing is absent from UKESM1. For further details on aerosols and clouds in UKESM1, see Mulcahy et al. (2020).

Both natural and anthropogenic SO_2 emissions are taken from the Coupled Model Intercomparison Project Phase 6 (CMIP6) inventory (Feng et al., 2020). In UKESM1, all anthropogenic SO_2 emissions are prescribed as a combined sum of the individual sources (e.g., shipping, energy, waste) with 2.5% emitted as primary SO_4^{2-}. These emissions are released within the first vertical level only at a height of 20 m above the surface. We run UKESM1 at a horizontal latitude-longitude resolution of 1.25° × 1.875° with 85 vertical levels that use terrain-following hybrid height coordinates and are capped at 85 km above sea level. In the ocean, a horizontal resolution of 1° and 75 vertical levels is used.

2.2. Experimental Design

Our study centers on two anthropogenic SO_2 emission profiles; a control profile identical to that constructed for the UKESM1 "middle-of-the-road" Shared Socioeconomic Pathway 2–4.5 (SSP2-4.5) scenario (O'Neill et al., 2016), and an IMO2020 profile in which the control profile emissions are reduced over ocean cells by 85.7% (percentage change of the new global limit on sulfur mass content relative to its predecessor). An exception is made for those ocean cells that reside within the IMO sulfur emission control areas as these regions are already subject to more stringent sulfur content limits and so unaffected by IMO2020. This method to replicate post-IMO2020 anthropogenic SO_2 emissions assumes that shipping is the only source over ocean, neglecting minor contributions from offshore platforms (∼1%–2%). The average annual reduction in the mass of anthropogenic SO_2 emissions in IMO2020 versus SSP2-4.5 from 2020 to 2029 inclusive is shown in Figure 1a. The spatial pattern of the reduction aligns with the major international shipping lanes. The largest reductions are in areas surrounding three of the world's busiest shipping routes—the Panama Canal, the Suez Canal and the Malacca Strait—with reductions exceeding 1.5 Kt of SO_2 for some grid cells. Outside these narrow passages, widespread reductions are found across the North Atlantic and North Pacific, experiencing mean annual reductions of 0.8 and 0.5 Mt of SO_2 respectively. South China Sea also experiences notable reductions in anthropogenic SO_2 emissions. Reductions are far lower in the Southern Hemisphere aside from a few well traveled routes. A time series of the global annual mass of shipping SO_2 emissions is depicted in Figure 1b showing an average annual decline of 9.9 Mt of SO_2 due to IMO2020 from Jan 2020 onwards; slightly higher than the predicted 8.5 Mt of SO_2 in Sofiev et al. (2018). This is likely due to differing underlying baseline emissions and assumed reductions, as well as our inadvertent reduction of other anthropogenic SO_2 sources (e.g., offshore platforms, coastal areas partially occupying ocean grid elements) due to how UKESM1 prescribes these emissions as a combined sum. Nevertheless, this reasonable agreement, and the spatial correlation with international shipping lanes, gives credence to our IMO2020 emission profile.

We compare the control surface SO_2 emission scenario to its IMO2020 counterpart using both fixed SST atmosphere-only experiments and coupled atmosphere-ocean experiments. The fixed SST atmosphere-only simulations are run for 10 years and use the observed SST and sea ice from 2005 to 2015, with land surface temperatures free to respond (e.g., Forster et al., 2016; Pincus et al., 2016). The control simulation set is

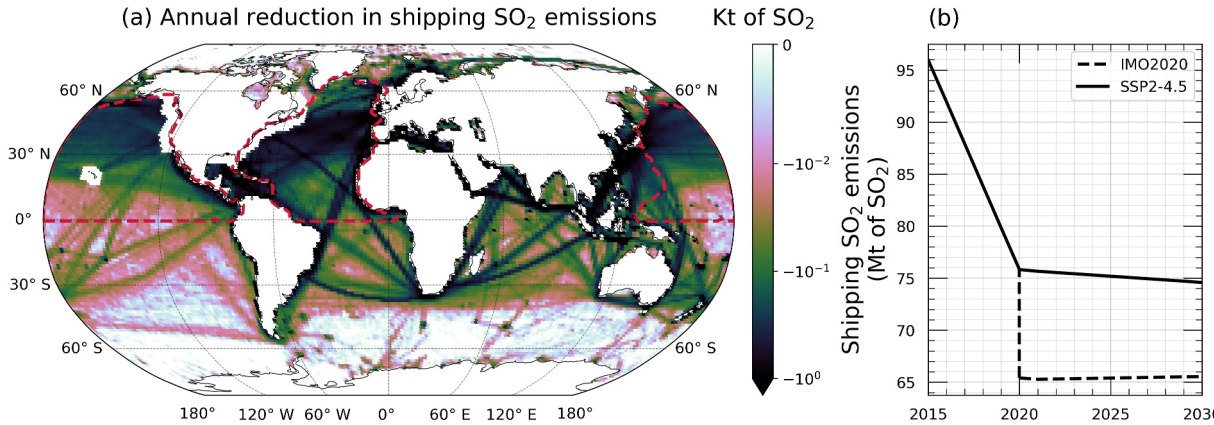

Figure 1. (a) Average annual reduction in the mass of anthropogenic SO_2 emissions due to the modeled impact of IMO2020 on SO_2 shipping emissions using UKESM1. Averages use annual values between 2020 and 2029 inclusive. We use the International Hydrographic Organization (IHO) North Atlantic and North Pacific boundaries in this study (red dashed lines) (Flanders Marine Institute, 2018). Note, sulfur emission control areas show no reduction (see text). (b) Global annual mass of shipping SO_2 emissions within the IMO2020 and control scenarios.

comprised of 10 ensemble members which have the surface SO_2 emissions set to that of SSP2-4.5 from 2020 to 2029 inclusive (solid line in Figure 1b), whilst the parallel perturbed set has the IMO2020 reduction in surface SO_2 emissions (dashed line in Figure 1b). This results in 100 years of simulation for both sets. Similarly, for the coupled atmosphere-ocean experiment, we perform two sets of parallel simulations using 16 SSP2-4.5 ensemble members from 2015 to 2029 inclusive. One set is prescribed with SSP2-4.5 surface SO_2 emissions, and another with the modified IMO2020 surface SO_2 emissions. For our analysis, only output from 2020 onwards is considered. Subsequently, from the 16 sets of paired simulations, we have 160 model years to identify a climate signal from IMO2020. The decision to consider only the impact on the decade immediately after IMO2020 follows the logic that the IMO2020 prompted reductions in SO_2 emissions will be inconsequential post-2030 as—at least in the favorable future climate scenarios—similar reductions will have been factored in by then; IMO2020 simply brought them forward.

3. Radiative Forcing Impact

We calculate the IMO2020 effective radiative forcing (ERF) from the difference in the net (shortwave, SW and longwave, LW) ToA radiative flux between our pairs of parallel fixed SST atmosphere-only simulations following the recommendations of Forster et al. (2016). Figure 2 depicts the average net ERF of the IMO2020 impact on SO_2 emissions, along with a decomposition of this ERF using the methodology of Ghan (2013). These individual components (which sum up to the total ERF) are the aerosol IRF, the change in cloud radiative effect (ΔCRE), and flux changes driven by clear-sky, non-aerosol (clear-clean) Radiative Adjustments (RA). A "local" null hypothesis is assessed at each grid element using the Wilcoxon signed-rank test. The overall expected proportion of "false positives" resulting from the amalgamation of these local null hypothesis tests is controlled at 5% using the False Discovery Method (FDR, Wilks, 2006, 2016). Stippling indicates the grid elements with null hypothesis rejections post-FDR adjustment. Summarizing values are provided in Table 1.

The overall impact of the SO_2 emissions reduction on global aerosol ERF is a warming of 0.139 ± 0.019 Wm^{-2}. The standard error of the model ensemble is used to estimate the uncertainty here and throughout this study. Generally, the positive ERF values coincide with areas of high shipping traffic, ergo large reductions in shipping emissions (e.g., North Atlantic, North-East Pacific, and Southeast Asia). Global aerosol IRF is 0.069 ± 0.003 Wm^{-2} and ΔCRE is 0.096 ± 0.014 Wm^{-2} which—as they act as proxies for the aerosol direct and indirect effects—suggest that, at the global scale, aerosol induced changes to cloud properties is the main mechanism behind the IMO2020 positive forcing; a result somewhat expected as the majority of the aerosol reduction will likely be underneath heavy, pre-existing cloud cover limiting ToA radiative flux changes from the aerosol direct effect. This aerosol-indirect effect dominance is evident regionally, such as in the North Atlantic and North Pacific, where ΔCRE is approximately 95% and 94% of the magnitude of the ERF here respectively. Although, in other regions the change in direct absorption and scattering of aerosol dominates the ACI forcing.

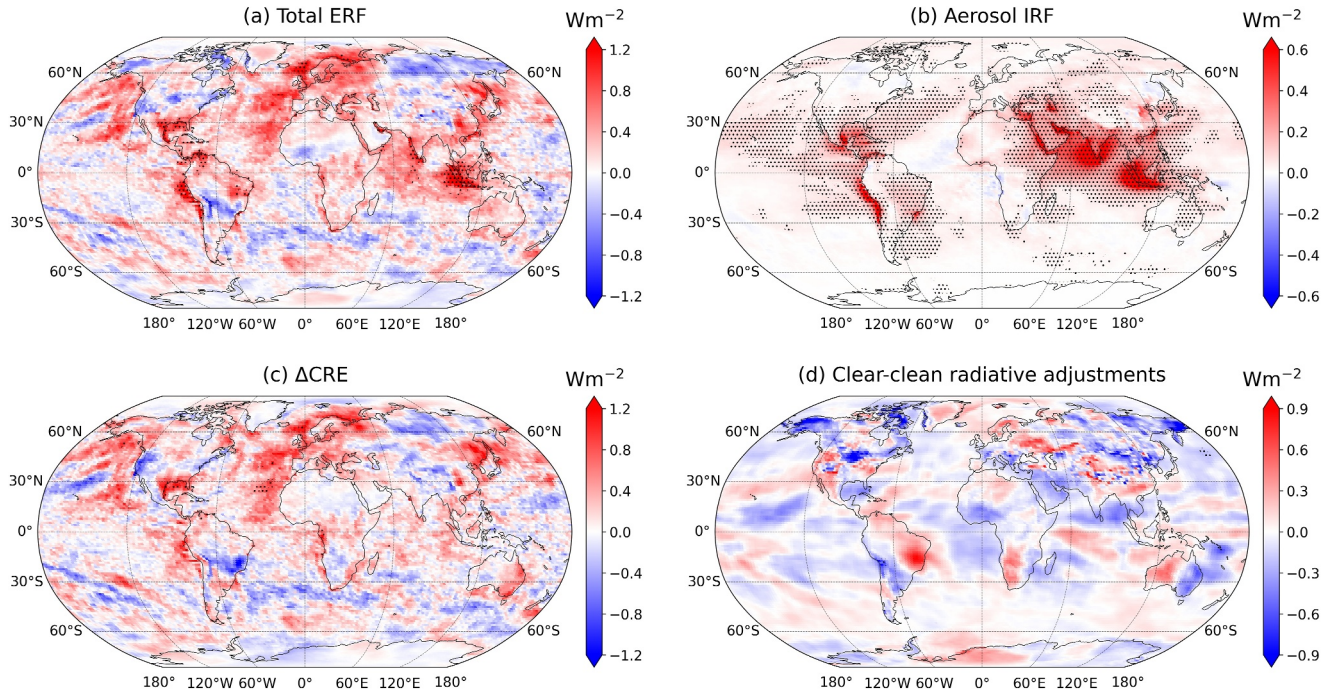

Figure 2. (a) IMO2020 net (shortwave, SW and longwave, LW) aerosol effective radiative forcing using UKESM1. Included are the contributions from: (b) the aerosol instantaneous radiative forcing, (c) the change in cloud radiative effect (ΔCRE), and (d) flux changes driven by clear-sky, non-aerosol (clear-clean) radiative adjustments. Values are averages across all years within the 10 fixed sea-surface temperature atmosphere-only paired simulations. Stippling highlights grid elements with null hypothesis rejections based on applying the False Discovery Method (FDR) at a 5% control level (see text). Global and regional values are provided in Table 1.

For example, aerosol IRF outweighs ΔCRE across the western coast of South America, the Caribbean Sea, the Red Sea, the North Indian Ocean, and parts of South East Asia. Globally, the clear-clean RA effect is a minor, though not negligible, negative forcing, with the strongest local changes found mainly within areas of North America and the Russian Far East that typically experience snow and ice cover. This indicates a likelihood that differences in snow cover strongly contribute to this term over the northern continents. Elsewhere, changes in atmospheric water vapor and temperature may dominate this clear-clean radiative component.

4. Coupled Atmosphere-Ocean Experiment

To assess the surface temperature and further understand the ToA radiation responses to IMO2020, we analyze two 16-member coupled atmosphere-ocean ensembles with and without the IMO2020 reduction in SO_2 emissions.

Table 1
IMO2020 Net (Shortwave, SW and Longwave, SW) Aerosol Effective Radiative Forcing, Aerosol Instantaneous Radiative Forcing, Change in Cloud Radiative Effect (ΔCRE), and Flux Changes Driven by Clear-Sky, Non-Aerosol (Clear-Clean) Radiative Adjustments Estimated Using UKESM1

Region	ERF (Wm^{-2})	Aerosol IRF (Wm^{-2})	ΔCRE (Wm^{-2})	Clear-clean RA (Wm^{-2})
Global	0.139 ± 0.019	0.069 ± 0.003	0.096 ± 0.014	−0.026 ± 0.013
N. Hemisphere	0.20 ± 0.03	0.094 ± 0.005	0.155 ± 0.018	−0.05 ± 0.02
S. Hemisphere	0.08 ± 0.03	0.045 ± 0.002	0.04 ± 0.02	0.00 ± 0.02
N. Atlantic	0.32 ± 0.05	0.040 ± 0.019	0.30 ± 0.06	−0.02 ± 0.03
N. Pacific	0.14 ± 0.05	0.059 ± 0.005	0.013 ± 0.05	−0.05 ± 0.03

Note. Values are averages across the 10 fixed-SST atmosphere-only ensemble members with the standard error used to quantify the uncertainty.

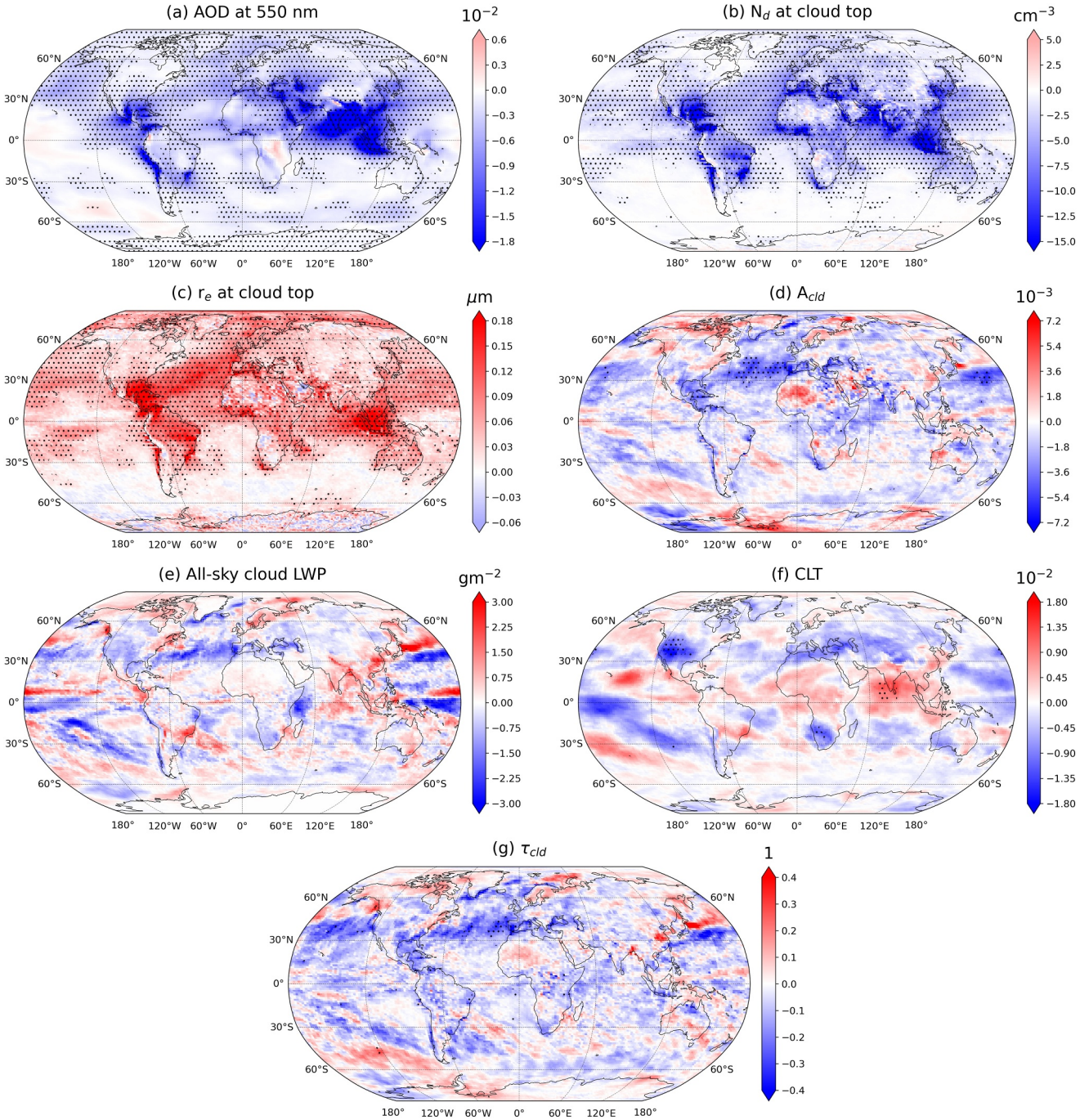

Figure 3. Anomalies in (a) aerosol optical depth at 550 nm, cloud top (b) droplet number concentration (N_d) and (c) droplet effect radius (r_e), (d) cloud albedo (A_{cld}), (e) all-sky liquid water path, (f) cloud fraction (CLT), and (g) cloud optical depth (τ_{cld}) due to IMO2020 using UKESM1. Values are averages from 2020 to 2029 inclusive across the 16 ensemble members. Stippling highlights grid elements with null hypothesis rejections based on applying the False Discovery Method (FDR) at a 5% control level (see text). Global and regional values are provided in Table 2.

4.1. Aerosol-Induced Cloud Adjustments

The ensemble-mean annual anomalies of aerosol optical depth (AOD) at 550 nm, cloud top N_d and r_e, and A_{cld} due to reduced SO_2 emissions following IMO2020 are shown in Figure 3a–3d, with summary values provided in Table 2. As before, stippling indicates grid elements with rejected null hypotheses after applying

Table 2
Anomalies in Aerosol and Cloud Properties Due to IMO2020 Using UKESM1

Region	AOD (10^{-2})	N_d (cm^{-3})	r_e (μm)	A_{cld} (10^{-3})	LWP (gm^{-2})	CLT (10^{-3})	τ_{cld} (10^{-2})
Global	−0.369 ± 0.018	−2.83 ± 0.06	0.0464 ± 0.0015	−0.57 ± 0.08	−0.06 ± 0.03	−0.6 ± 0.2	−3.4 ± 0.3
N. Hemisphere	−0.54 ± 0.03	−3.99 ± 0.08	0.0622 ± 0.0019	−0.78 ± 0.15	−0.02 ± 0.04	−0.5 ± 0.4	−4.3 ± 0.5
S. Hemisphere	−0.203 ± 0.015	−1.67 ± 0.07	0.031 ± 0.002	−0.35 ± 0.09	−0.09 ± 0.06	−0.7 ± 0.4	−2.5 ± 0.4
N. Atlantic	−0.40 ± 0.07	−4.3 ± 0.2	0.090 ± 0.005	−1.8 ± 0.3	−0.33 ± 0.11	0.1 ± 0.8	−8.7 ± 1.4
N. Pacific	−0.32 ± 0.03	−2.03 ± 0.17	0.046 ± 0.004	−0.91 ± 0.18	−0.03 ± 0.13	−0.9 ± 0.8	−5.4 ± 0.9

Note. Values are averages from 2020 to 2029 inclusive across the 16 coupled atmosphere-ocean ensemble members with the standard error used to quantify the uncertainty.

the FDR method at 5%. We simulate a global decrease in AOD of $-0.369 \pm 0.018 \times 10^{-2}$, approximately 3% of the 2020–2029 control average, which is a likely consequence of a reduction in aerosol concentrations, specifically SO_4^{2-} (not shown here). The largest reductions are centered around three of the world's busiest shipping routes—the Panama Canal, the Suez Canal, and the Malacca Strait—where reductions exceed 0.015. Outside of these narrow shipping passages, we note extensive reductions in AOD across the oceans of the Northern Hemisphere and areas off the coast of South America. Interestingly, despite very limited shipping traffic, Antarctica displays a significant AOD response. However, as sea-salt and dimethyl sulfide (DMS) aerosol are dependent on wind speed in UKESM1, it's likely these significant changes arise due to differences in wind speed between our paired simulations in a pristine environment as opposed to a direct consequence of IMO2020.

Decreasing aerosol concentration is expected to lead to decreases in the number of available CCN and, subsequently, N_d. Here we find that IMO2020 leads to a global decrease in cloud top N_d of -2.83 ± 0.06 cm^{-3}, with a spatial pattern visibly similar to that of AOD. Of note is the decrease of -4.3 ± 0.2 cm^{-3} modeled in the North Atlantic, roughly a 5% reduction relative to a world without IMO2020. In terms of cloud top r_e, our simulations estimate a global increase of 0.0464 ± 0.0015 µm, with a spatial pattern comparable to that of AOD and N_d. These increases are predominantly across the Northern Hemisphere oceans and select areas within 0–30°S. The spatially correlated changes in AOD, N_d, and r_e follow the spatial pattern of the shipping emission reductions, though with less definition likely due to the dispersion of SO_2 and the subsequent SO_4^{-2}, suggesting that IMO2020 regulations are causing aerosol-induced cloud changes to droplet concentration and size. However, only in the North Atlantic and North Pacific do these mircophysical changes align with a significant decrease in A_{cld}, thus exhibiting a complete Twomey effect "chain"—albeit reversed as here aerosol is removed rather than added. Further macrophysical cloud properties, namely liquid water path, cloud fraction (CLT), and cloud optical depth (τ_{cld}), are listed in Table 2, and all decrease at the global scale in agreement with the theorised second aerosol indirect effects via precipitation suppression. However, as evident in Figures 3e–3g, the signal-to-noise ratio is too low and a larger ensemble is required to robustly connect these possible changes to IMO2020.

4.2. Surface Temperature Response

The ensemble-mean annual near-surface (1.5 m) air temperature (T_{as}) anomaly across the current decade due to IMO2020 restrictions on shipping emissions is shown in Figure 4a. As with previous spatial figures, stippling indicates grid elements with rejected null hypotheses after applying the FDR method at 5%. Our simulations suggests a 2020–2029 mean global annual warming of 0.046 ± 0.010 °C which is mainly caused by large, positive regional responses. For instance, noticeable warming occurs in the North Atlantic, North and South-East Pacific, and the Caribbean Sea—areas with both significant warming ERF and cloud albedo increases. We note a hemispheric contrast of 0.067 ± 0.017 °C, with 0.079 ± 0.013 °C warming in the Northern hemisphere and 0.012 ± 0.011 °C warming in the Southern hemisphere. Interestingly, although the North Indian ocean and West coast of South America exhibit a significant positive forcing due to large aerosol IRF, they do not display a response in T_{as}. Figures 4b–4f presents a comparison of global and regional

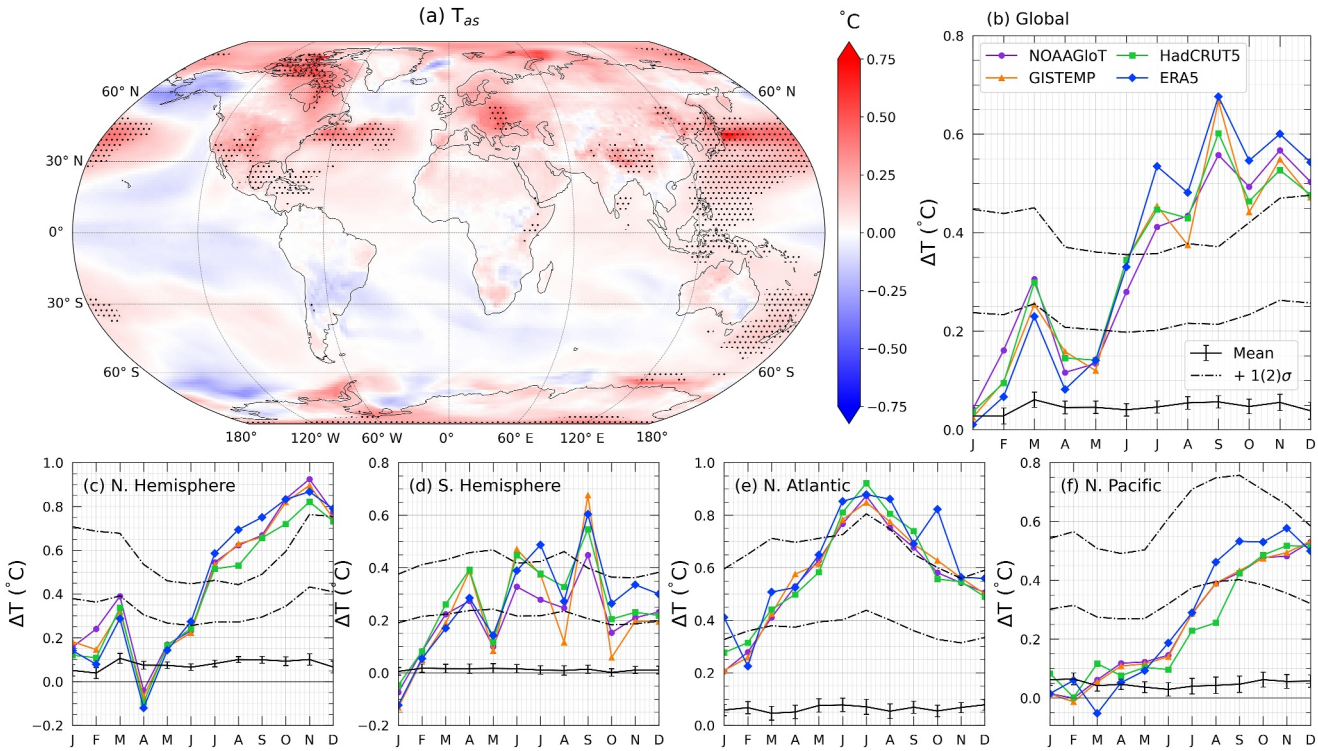

Figure 4. (a) Ensemble-mean annual near-surface temperature (T_{as}) anomaly due to IMO2020 using UKESM1. Values are averages of 2020–2029 inclusive across the 16 ensemble members. Stippling highlights grid elements with null hypothesis rejections based on applying the False Discovery Method (FDR) at a 5% control level (see text). Global and regional values are provided in Table 3 (b–f) Global and regional observed 2023 T_{as} anomalies relative to a 2012–2019 baseline from NOAAGlobalTemp version 6, GISTEMP version 4, HadCRUT5, and ERA5, alongside the associated monthly variability in the 2020–2029 ensemble-mean T_{as} response due to IMO2020. Error bars and dashed lines depict the standard error and positive standard deviations (+1 and +2 σ) of the modeled IMO2020 monthly values respectively.

observed 2023 T_{as} anomalies relative to a 2012–2019 baseline from NOAAGlobalTemp version 6 (Huang et al., 2020), GISTEMP version 4 (Lenssen et al., 2019), HadCRUT5 (Morice et al., 2021), and ERA5 (Hersbach et al., 2020) data sets, alongside the associated 2020–2029 ensemble-mean T_{as} response to IMO2020 with one and two positive standard deviations of the monthly anomalies depicted. Both globally and regionally, IMO2020 helps to explain the exceptional warmth in 2023, although the proportion of this warming that the shipping regulations can account for is uncertain due to the high natural variability in our model ensemble. For example, the vast majority of North Atlantic and North Pacific warming is explained by IMO2020 in the model realizations with the stronger responses, yet the mean response suggests only a minor contribution. However, even in these strong response model realizations, globally other factors alongside IMO2020 are needed to fully account for the observed T_{as} from July–December 2023.

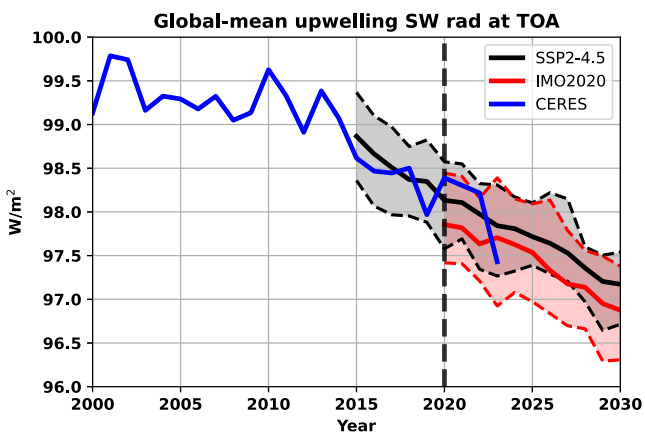

Figure 5. Global-mean upwelling shortwave (SW) radiation at the top-of-atmosphere (ToA) from the "Clouds and the Earth's Radiant Energy System" project (CERES) observations (blue), and the SSP2-4.5 (black), and IMO2020 (red) ensembles. The thick lines show the ensemble-mean, while the dashed lines show the ensemble minimum and maximum for each month.

4.3. Top-of-Atmosphere Shortwave Response

The ToA upwelling SW radiation is shown in Figure 5. The observations are from the "Clouds and the Earth's Radiant Energy System" project (CERES, Loeb et al., 2018), and show a decline in upwelling ToA SW radiation. Hodnebrog et al. (2024) (their Figure 2b) attribute more than half of this SW trend in 2001–2019 to the ERF from a decline in anthropogenic aerosol emissions. Figure 5 also shows the SSP2-4.5 ensemble-mean in upwelling

Table 3
Anomalies in Top-of-Atmosphere (ToA) Radiative Fluxes (Shortwave, SW and Net) and Near-Surface Temperature (T_{as}) Due to IMO2020 Using UKESM1

Region	ToA SW (Wm^{-2})	ToA Net (Wm^{-2})	T_{as} (°C)
Global	0.25 ± 0.02	0.13 ± 0.03	0.046 ± 0.010
N. Hemisphere	0.35 ± 0.04	0.19 ± 0.04	0.079 ± 0.013
S. Hemisphere	0.16 ± 0.04	0.07 ± 0.03	0.012 ± 0.011
N. Atlantic	0.40 ± 0.08	0.24 ± 0.07	0.064 ± 0.018
N. Pacific	0.28 ± 0.10	0.13 ± 0.10	0.049 ± 0.019

Note. Values are averages of 2020–2029 inclusive across the 16 coupled atmosphere-ocean ensemble members with the standard error used to quantify the uncertainty.

ToA SW radiation (black) as well as the IMO2020 ensemble-mean (red). The dashed lines show the ensemble minimum and maximum for each month. The global and regional values of the change in ToA SW and net radiation are summarized in Table 3. The year 2023 saw a large decline in upwelling ToA SW radiation, which may help to explain the unprecedented temperature increase of that year. These results show that this decline is within the variability of the SSP2-4.5 ensemble (i.e., without shipping emission reductions), but was made more likely by the IMO2020 regulations. Furthermore, the variability in upwelling ToA SW radiation, assessed here as being the difference between the monthly minimum and maximum, is noticeably larger in the IMO2020 simulations than in the reference SSP2-4.5 simulations. We speculate that this may be due to a higher sensitivity to the variability in natural aerosol emissions over oceans in the absence of anthropogenic aerosol emissions. For example, Figure 6 in Jin et al. (2018) show that the CRE of shipping emissions is a factor of 2 larger when the oceanic phytoplankton-derived DMS emissions are set to half of their reference value ("DMSLow") (Figure 4).

5. Discussion and Conclusions

Prompting a rise in cleaner marine fuels at the turn of the decade, IMO2020 has caused an abrupt reduction in anthropogenic SO_2 emissions. Here we use UKESM1 simulations to show that this regulation has inadvertently produced small, yet discernible, climatic impacts, particularly across regions with high shipping traffic. We estimate a radiative forcing change of 0.139 ± 0.019 Wm^{-2} due to this decline in shipping emissions which is in agreement with recent studies (Diamond, 2023; Skeie et al., 2024; Yoshioka et al., 2024; Yuan et al., 2024). We disentangle this forcing into its individual components, finding that the predominant factor is the aerosol-induced changes in the cloud radiative effect rather than changes to the direct scattering and absorption of the aerosol itself, particularly across the Northern Hemisphere oceans. By assessing the cloud micro- and macrophysical properties, we find that the Twomey effect is likely the driver of this cloud forcing in these regions, with little contribution from further second aerosol-indirect effects. These instance of localized forcings align well with strong T_{as} responses, which contribute to our overall IMO2020 modeled global annual mean warming of 0.046 ± 0.010°C; approximately 2–3 years of global warming (Forster et al., 2024).

In relation to the record warming observed in 2023—whilst it is within the variability of our model ensemble that IMO2020 could account for the majority of the North Atlantic and North Pacific warming—at the global scale we suggest IMO2020 provides only a minor contribution given that even the highest responses from our model ensemble would not be able to fully account for the 2023 temperatures. This poses the question as to what has caused the warming. Some propose the Hunga Tonga-Hunga Ha'apai eruption in the South Pacific as a contributor, citing studies suggesting the mass injection of water into the stratosphere has caused warming at the surface (Jenkins et al., 2023; Millán et al., 2022; Sellitto et al., 2022), yet this net warming is contested by others due to the cooling effect from the increased formation of SO_4^{2-} due to this additional water vapor (Schoeberl et al., 2023). However, even combining the upper estimate of +0.035°C from Jenkins et al. (2023), with our IMO2020 warming does not replicate the 2023 magnitudes. It is also worth noting that 2023 was characterized by a record low amount of reflected solar radiation. In this work, we show that this decline is within the variability of the simulations without the reduction in shipping emissions, but was made more likely by the IMO2020 regulations. Furthermore, the variability in reflected solar radiation is noticeably larger in the IMO2020 simulations compared to the reference simulations, which we speculate is due to a higher sensitivity to the variability in natural aerosol emissions over oceans in the absence of shipping emissions.

Whilst our modeled warming caused by IMO2020 may appear small in comparison with 2023, it will be persistent across the current decade and so should be viewed as an additional warming to long-term climate change targets such as the 1.5°C goal of the Paris Agreement. For example, Forster et al. (2024) states that 2014–2023 was 1.19°C relative to the pre-industrial, thus adding our 2020–2029 IMO2020 ensemble-mean

warming to this would leave 0.26°C before this notable target is surpassed. In addition, we can estimate the cumulative expected warming to have occurred following a given number of years since the IMO2020 introduction. Due to the small signal associated with the modeled IMO2020 impact, we use a recent UKESM1 marine cloud brightening (MCB) experiment with larger aerosol perturbations to do so, assuming the temperature response across the same timescale (i.e., a decade) is the same for marine clouds that are brightened with sea-salt rather than SO_4^{2-} (see Supplementary Information). These estimates suggest that at the end of 2023, 0.040°C of warming will have occurred due to IMO2020, representing 58.0% of the total warming expected by the end of the decade (0.069°C), or 87.0% of the ensemble-mean annual warming across 2020–2029. To verify this estimate would require increasing our model ensemble in order to isolate the temperature response of IMO2020 years-by-year. Nevertheless, the possibility that over half the IMO2020 warming expected this decade has already been realised increases pressure on our remaining carbon budget.

It must be acknowledged that this study solely relies on model simulations to assess IMO2020 and so our analysis is subject to certain assumptions and limitations. For example, our experimental set-up assumes shipping emissions are released 20 m above mean sea level, whilst real-world values are more likely 40–50 m (Gan et al., 2023), and lacks explicit representations of the resulting plume rise. Subsequently, as SO_2 removal via dry deposition is more efficient closer to the surface in UKESM1 (Mulcahy et al., 2020), our SO_2 burden is likely underestimated which, in turn, may mean our cooling effect and temperature response are also. Similarly, studies have proposed that the aerosol-induced cloud cover response is too weak in general circulation models (Chen et al., 2022, 2024), which again implies that the IMO2020 warming estimate here is too conservative. On the other hand, UKESM1 is unable to explicitly simulate ship tracks and this inability has been suggested to cause up to a $\sim$ 50% overestimation in the cloud radiative effect of low-level marine clouds (Possner et al., 2016) which, coupled with the reported high climate sensitivity of UKESM1 (Andrews et al., 2019), suggests that the IMO2020 warming is less than the amount proposed here. Other model limitations include a low signal-to-noise ratio, the absence of aerosol or N_d in the UKESM1 convective cloud scheme meaning a convective forcing component is missing, uncertainty in the real-world reduction to SO_2 from shipping emissions (we assume ships pre-IMO2020 were using fuels at the legal maximum limit of 3.5% sulfur), and neglecting any reduction in other pollutants present in shipping exhaust fumes (nitrogen oxides, black carbon, particulate matter etc.). Naturally, using observations removes these limitations, yet a longer observational record than the current one would be needed to fully isolate the IMO2020 signal from natural variability and other confounding influences (e.g., COVID-19). Until such time, the community will continue to rely on modeling studies and so should potentially look toward a model intercomparison project to mitigate this uncertainty.

IMO2020 is likely already impacting our climate, and will continue to do so this decade, via direct and indirect aerosol processes. The recent extremes are perhaps too large to solely attribute to IMO2020, yet the warming impact of IMO2020 is appreciable enough to warrant inclusion in updates to long-term climate targets and remaining carbon budgets. The newly enforced SO_2 emissions restrictions are perhaps the first large-scale geoengineering experiment—albeit inadvertent and "reversed"—and may play a pivotal role in the study of MCB as a climate intervention technique (e.g., Feingold et al., 2024; Haywood et al., 2023; Yuan et al., 2024).

Appendix A: Shipping SO_2 Radiative Forcing Estimates

Estimates of the radiative forcing from shipping emissions of SO_2 in the literature are provided in Table A1. These estimates are derived from varying methodologies and assumptions, so caution should be exercised when drawing comparisons.

Table A1
Estimates of the Radiative Forcing From Shipping Emissions of SO_2 in the Literature. These Estimates are Made Using Very Different Methods and Assumptions, so Caution Should Be Used When Comparing Them

Reference	Model	Forcing estimate (Wm^{-2})	Perturbation
Jordan and Henry	UKESM1	0.139	85.7% reduction
Quaglia and Visioni (2024)	CESM2	0.14	90% reduction
Skeie et al. (2024)	CESM2	0.085	80% reduction
Skeie et al. (2024)	ModelE_MATRIX	0.065	80% reduction
Skeie et al. (2024)	ModelE_OMA	0.08	80% reduction
Skeie et al. (2024)	NORESM2	0.065	80% reduction
Skeie et al. (2024)	OsloCTM3	0.07	80% reduction
Yuan et al. (2024)	GEOS-GOCART	0.2	85% reduction
Yoshioka et al. (2024)	HadGEM-GC3.1	0.13	80% reduction
Diamond (2023)	Kriging method	$\mathcal{O}(0.1)$	Satellite retrievals
Yuan et al. (2022)	Machine learning model	0.02–0.27	Satellite retrievals
Bilsback et al. (2020)	GEOS-Chem	0.027	85% reduction
Jin et al. (2018)	CESM1.2.2	0.153–0.255	All shipping emissions
Sofiev et al. (2018)	FMI SILAM	0.071	75% reduction
Partanen et al. (2013)	ECHAM5.5	0.33	85% reduction
Peters et al. (2013)	ECHAM-HAM	0.1–0.46	All shipping emissions
Righi et al. (2011)	EMAC-MADE	0.28–0.40	All shipping emissions
Lauer et al. (2009)	ECHAM5/MESSy1-MADE	0.3–0.313	81.5% reduction
Schreier et al. (2007)	Visual analysis	0.004–0.006	Satellite retrievals
Capaldo et al. (1999)	GFDL chemical transport model	0.11	All shipping emissions

Data Availability Statement

The UKESM1 simulation data used in this study are available at Zenodo via https://doi.org/10.5281/zenodo.11504280 (Jordan, 2024). All observational data sets used in this study are publicly available. NOAAGlobalTemp data are available via https://www.ncei.noaa.gov/products/land-based-station/noaa-global-temp (Huang et al., 2020). GISTEMP data are available via https://data.giss.nasa.gov/gistemp/ (Lenssen et al., 2019). HadCRUT5 data are available via https://www.metoffice.gov.uk/hadobs/hadcrut5/ (Morice et al., 2021). ERA5 data are available via https://www.ecmwf.int/en/forecasts/dataset/ecmwf-reanalysis-v5 (Hersbach et al., 2020). CERES data are available via https://ceres.larc.nasa.gov/data/ (Loeb et al., 2018). The marine boundaries used in this study are produced by the Flanders Marine Institute and available via https://doi.org/10.14284/323 (Flanders Marine Institute, 2018). The code used to produce the results presented in this study is available at Zenodo via https://zenodo.org/doi/10.5281/zenodo.13150210 (Jordan & Henry, 2024).

Acknowledgments
The authors would like to express their gratitude to Andy Jones, Ben Johnson, and Jim Haywood for providing their support in this work. Further appreciation to Andy Jones for sharing the UKESM1 MCB experiment results. GJ is supported by the Met Office Hadley Centre Climate Programme funded by DSIT. MH is funded by SilverLining through their Safe Climate Research Initiative.

References

Abdul-Razzak, H., & Ghan, S. J. (2000). A parameterization of aerosol activation: 2. Multiple aerosol types. *Journal of Geophysical Research*, *105*(D5), 6837–6844. https://doi.org/10.1029/1999JD901161

Ackerman, A., Kirkpatrick, M., Stevens, D., & Toon, O. (2004). The impact of humidity above stratiform clouds on indirect aerosol climate forcing. *Nature*, *432*(7020), 1014–1017. https://doi.org/10.1038/nature03174

Albrecht, B. A. (1989). Aerosols, cloud microphysics, and fractional cloudiness. *Science*, *245*(4923), 1227–1230. https://doi.org/10.1126/science.245.4923.1227

Andrews, T., Andrews, M. B., Bodas-Salcedo, A., Jones, G. S., Kuhlbrodt, T., Manners, J., et al. (2019). Forcings, feedbacks, and climate sensitivity in HadGEM3-GC3.1 and UKESM1. *Journal of Advances in Modeling Earth Systems*, *11*(12), 4377–4394. https://doi.org/10.1029/2019MS001866

Archibald, A. T., O'Connor, F. M., Abraham, N. L., Archer-Nicholls, S., Chipperfield, M. P., Dalvi, M., et al. (2020). Description and evaluation of the UKCA stratosphere–troposphere chemistry scheme (StratTrop vn 1.0) implemented in UKESM1. *Geoscientific Model Development*, *13*(3), 1223–1266. https://doi.org/10.5194/gmd-13-1223-2020

Bellouin, N., Quaas, J., Gryspeerdt, E., Kinne, S., Stier, P., Watson-Parris, D., et al. (2020). Bounding global aerosol radiative forcing of climate change. *Reviews of Geophysics*, *58*(1), e2019RG000660. https://doi.org/10.1029/2019RG000660

Best, M. J., Pryor, M., Clark, D. B., Rooney, G. G., Essery, R. L. H., Ménard, C. B., et al. (2011). The joint UK land environment simulator (JULES), model description – Part 1: Energy and water fluxes. *Geoscientific Model Development*, *4*(3), 677–699. https://doi.org/10.5194/gmd-4-677-2011

Bilsback, K. R., Kerry, D., Croft, B., Ford, B., Jathar, S. H., Carter, E., et al. (2020). Beyond SOx reductions from shipping: Assessing the impact of NOx and carbonaceous-particle controls on human health and climate. *Environmental Research Letters*, *15*(12), 124046. https://doi.org/10.1088/1748-9326/abc718

Bretherton, C. S., Blossey, P. N., & Uchida, J. (2007). Cloud droplet sedimentation, entrainment efficiency, and subtropical stratocumulus albedo. *Geophysical Research Letters*, *34*(3). https://doi.org/10.1029/2006GL027648

Capaldo, K., Corbett, J. J., Kasibhatla, P., Fischbeck, P., & Pandis, S. N. (1999). Effects of ship emissions on sulphur cycling and radiative climate forcing over the ocean. *Nature*, *400*(6746), 743–746. https://doi.org/10.1038/23438

Chen, Y., Haywood, J., Wang, Y., Malavelle, F., Jordan, G., Partridge, D., et al. (2022). Machine learning reveals climate forcing from aerosols is dominated by increased cloud cover. *Nature Geoscience*, *15*(8), 609–614. https://doi.org/10.1038/s41561-022-00991-6

Chen, Y., Haywood, J., Wang, Y., Malavelle, F., Jordan, G., Peace, A., et al. (2024). Substantial cooling effect from aerosol-induced increase in tropical marine cloud cover. *Nature Geoscience*, *17*(5), 1–7. https://doi.org/10.1038/s41561-024-01427-z

Chu Van, T., Ramirez, J., Rainey, T., Ristovski, Z., & Brown, R. J. (2019). Global impacts of recent IMO regulations on marine fuel oil refining processes and ship emissions. *Transportation Research Part D: Transport and Environment*, *70*, 123–134. https://doi.org/10.1016/j.trd.2019.04.001

Contini, D., & Merico, E. (2021). Recent advances in studying air quality and health effects of shipping emissions. *Atmoshpere*, *12*(1), 92. https://doi.org/10.3390/atmos12010092

Diamond, M. S. (2023). Detection of large-scale cloud microphysical changes within a major shipping corridor after implementation of the International Maritime Organization 2020 fuel sulfur regulations. *Atmospheric Chemistry and Physics*, *23*(14), 8259–8269. https://doi.org/10.5194/acp-23-8259-2023

Eyring, V., Isaksen, I. S., Berntsen, T., Collins, W. J., Corbett, J. J., Endresen, O., et al. (2010). Transport impacts on atmosphere and climate: Shipping. *Atmospheric Environment*, *44*(37), 4735–4771. https://doi.org/10.1016/j.atmosenv.2009.04.059

Faber, J., Hanayama, S., Zhang, S., Pereda, P., Comer, B., Hauerhof, E., et al. (2021). *Fourth IMO GHG study 2020 full report (Tech. Rep.)*. International Maritime Organization.

Feingold, G., Ghate, V. P., Russell, L. M., Blossey, P., Cantrell, W., Christensen, M. W., et al. (2024). Physical science research needed to evaluate the viability and risks of marine cloud brightening. *Science Advances*, *10*(12), eadi8594. https://doi.org/10.1126/sciadv.adi8594

Feng, L., Smith, S. J., Braun, C., Crippa, M., Gidden, M. J., Hoesly, R., et al. (2020). The generation of gridded emissions data for CMIP6. *Geoscientific Model Development*, *13*(2), 461–482. https://doi.org/10.5194/gmd-13-461-2020

Flanders Marine Institute. (2018). IHO sea areas [Dataset]. *Flanders Marine Institute*. https://doi.org/10.14284/323

Forster, P. M., Richardson, T., Maycock, A. C., Smith, C. J., Samset, B. H., Myhre, G., et al. (2016). Recommendations for diagnosing effective radiative forcing from climate models for CMIP6. *Journal of Geophysical Research: Atmospheres*, *121*(20), 12–460. https://doi.org/10.1002/2016JD025320

Forster, P. M., Smith, C., Walsh, T., Lamb, W. F., Lamboll, R., Hall, B., et al. (2024). Indicators of global climate change 2023: Annual update of key indicators of the state of the climate system and human influence. *Earth System Science Data*, *16*(6), 2625–2658. https://doi.org/10.5194/essd-16-2625-2024

Gan, L., Lu, T., & Shu, Y. (2023). Diffusion and superposition of ship exhaust gas in port area based on Gaussian puff model: A case study on Shenzhen port. *Journal of Marine Science and Engineering*, *11*(22), 330. https://doi.org/10.3390/jmse11020330

Ghan, S. J. (2013). Technical note: Estimating aerosol effects on cloud radiative forcing. *Atmospheric Chemistry and Physics*, *13*(19), 9971–9974. https://doi.org/10.5194/acp-13-9971-2013

Hansen, J. E., Sato, M., Simons, L., Nazarenko, L. S., Sangha, I., Kharecha, P., et al. (2023). Global warming in the pipeline. *Oxford Open Climate Change*, *3*(1), kgad008. https://doi.org/10.1093/oxfclm/kgad008

Hassellöv, I.-M., Turner, D. R., Lauer, A., & Corbett, J. J. (2013). Shipping contributes to ocean acidification. *Geophysical Research Letters*, *40*(11), 2731–2736. https://doi.org/10.1002/grl.50521

Haywood, J. M., Jones, A., Jones, A. C., Halloran, P., & Rasch, P. J. (2023). Climate intervention using Marine Cloud Brightening (MCB) compared with Stratospheric Aerosol Injection (SAI) in the UKESM1 climate model. *Atmospheric Chemistry and Physics*, *23*(24), 15305–15324. https://doi.org/10.5194/acp-23-15305-2023

Hersbach, H., Bell, B., Berrisford, P., Hirahara, S., Horányi, A., Muñoz-Sabater, J., et al. (2020). The ERA5 global reanalysis. *Quarterly Journal of the Royal Meteorological Society*, *146*(730), 1999–2049. https://doi.org/10.1002/qj.3803

Hodnebrog, Ø., Myhre, G., Jouan, C., Andrews, T., Forster, P., Jia, H., et al. (2024). Recent reductions in aerosol emissions have increased Earth's energy imbalance. *Communications Earth & Environment*, *5*(166), 166. https://doi.org/10.1038/s43247-024-01324-8

Huang, B., Menne, M. J., Boyer, T., Freeman, E., Gleason, B. E., Lawrimore, J. H., et al. (2020). Uncertainty estimates for sea surface temperature and land surface air temperature in NOAAGlobalTemp version 5. *Journal of Climate*, *33*(4), 1351–1379. https://doi.org/10.1175/JCLI-D-19-0395.1

IMO. (2019). *IMO 2020: Consistent implementation of MARPOL annex VI*. International Martitime Organization (IMO).

Jägerbrand, A. K., Brutemark, A., Svedén, J. B., & Gren, I.-M. (2019). A review on the environmental impacts of shipping on aquatic and nearshore ecosystems. *Science of the Total Environment*, *695*, 133637. https://doi.org/10.1016/j.scitotenv.2019.133637

Jenkins, S., Smith, C., Allen, M., & Grainger, R. (2023). Tonga eruption increases chance of temporary surface temperature anomaly above 1.5°c. *Nature Climate Change*, *13*(2), 127–129. https://doi.org/10.1038/s41558-022-01568-2

Jin, Q., Grandey, B. S., Rothenberg, D., Avramov, A., & Wang, C. (2018). Impacts on cloud radiative effects induced by coexisting aerosols converted from international shipping and maritime DMS emissions. *Atmospheric Chemistry and Physics*, *18*(22), 16793–16808. https://doi.org/10.5194/acp-18-16793-2018

Jordan, G. (2024). IMO2020 UKESM1 fixed-SST atmosphere-only and coupled atmosphere-ocean experiments [Dataset]. *Zenodo*. https://doi.org/10.5281/zenodo.11504280

Jordan, G., & Henry, M. (2024). Code for "IMO2020 regulations accelerate global warming by up to 3 Years in UKESM1. [Code]. *Zenodo*. https://doi.org/10.5281/zenodo.13150210

Khairoutdinov, M., & Kogan, Y. (2000). A new cloud physics parameterization in a large-eddy simulation model of marine stratocumulus. *Monthly Weather Review*, *128*(1), 229–243. https://doi.org/10.1175/1520-0493(2000)128⟨0229:ANCPPI⟩2.0.CO;2

Kuhlbrodt, T., Jones, C. G., Sellar, A., Storkey, D., Blockley, E., Stringer, M., et al. (2018). The low-resolution version of HadGEM3 GC3.1: Development and evaluation for global climate. *Journal of Advances in Modeling Earth Systems*, *10*(11), 2865–2888. https://doi.org/10.1029/2018MS001370

Kuittinen, N., Jalkanen, J.-P., Alanen, J., Ntziachristos, L., Hannuniemi, H., Johansson, L., et al. (2021). Shipping remains a globally significant source of anthropogenic PN emissions even after 2020 sulfur regulation. *Environmental Science & Technology*, *55*(1), 129–138. https://doi.org/10.1021/acs.est.0c03627

Lauer, A., Eyring, V., Corbett, J. J., Wang, C., & Winebrake, J. J. (2009). Assessment of near-future policy instruments for oceangoing shipping: Impact on atmospheric aerosol burdens and the Earth's radiation budget. *Environmental Science & Technology*, *43*(15), 5592–5598. https://doi.org/10.1021/es900922h

Lenssen, N. J. L., Schmidt, G. A., Hansen, J. E., Menne, M. J., Persin, A., Ruedy, R., & Zyss, D. (2019). Improvements in the GISTEMP uncertainty model. *Journal of Geophysical Research: Atmospheres*, *124*(12), 6307–6326. https://doi.org/10.1029/2018JD029522

Loeb, N. G., Doelling, D. R., Wang, H., Su, W., Nguyen, C., Corbett, J. G., et al. (2018). Clouds and the Earth's Radiant Energy System (CERES) Energy Balanced and Filled (EBAF) top-of-atmosphere (TOA) Edition-4.0 data product. *Journal of Climate*, *31*(2), 895–918. https://doi.org/10.1175/jcli-d-17-0208.1

Mann, G. W., Carslaw, K. S., Ridley, D. A., Spracklen, D. V., Pringle, K. J., Merikanto, J., et al. (2012). Intercomparison of modal and sectional aerosol microphysics representations within the same 3-D global chemical transport model. *Atmospheric Chemistry and Physics*, *12*(10), 4449–4476. https://doi.org/10.5194/acp-12-4449-2012

Mann, G. W., Carslaw, K. S., Spracklen, D. V., Ridley, D. A., Manktelow, P. T., Chipperfield, M. P., et al. (2010). Description and evaluation of GLOMAP-mode: A modal global aerosol microphysics model for the UKCA composition-climate model. *Geoscientific Model Development*, *3*(2), 519–551. https://doi.org/10.5194/gmd-3-519-2010

Millán, L., Santee, M. L., Lambert, A., Livesey, N. J., Werner, F., Schwartz, M. J., et al. (2022). The Hunga Tonga-Hunga Ha'apai hydration of the stratosphere. *Geophysical Research Letters*, *49*(13), e2022GL099381. https://doi.org/10.1029/2022GL099381

Morcrette, C. J. (2012). Improvements to a prognostic cloud scheme through changes to its cloud erosion parametrization. *Atmospheric Science Letters*, *13*(2), 95–102. https://doi.org/10.1002/asl.374

Morice, C. P., Kennedy, J. J., Rayner, N. A., Winn, J. P., Hogan, E., Killick, R. E., et al. (2021). An updated assessment of near-surface temperature change from 1850: The HadCRUT5 data set. *Journal of Geophysical Research: Atmospheres*, *126*(3), e2019JD032361. https://doi.org/10.1029/2019JD032361

Mueller, N., Westerby, M., & Nieuwenhuijsen, M. (2023). Health impact assessments of shipping and port-sourced air pollution on a global scale: A scoping literature review. *Environmental Research*, *216*, 114460. https://doi.org/10.1016/j.envres.2022.114460

Mulcahy, J. P., Johnson, C., Jones, C. G., Povey, A. C., Scott, C. E., Sellar, A., et al. (2020). Description and evaluation of aerosol in UKESM1 and HadGEM3-GC3.1 CMIP6 historical simulations. *Geoscientific Model Development*, *13*(12), 6383–6423. https://doi.org/10.5194/gmd-13-6383-2020

Myhre, G., Samset, B. H., Schulz, M., Balkanski, Y., Bauer, S., Berntsen, T. K., et al. (2013). Radiative forcing of the direct aerosol effect from AeroCom Phase II simulations. *Atmospheric Chemistry and Physics*, *13*(4), 1853–1877. https://doi.org/10.5194/acp-13-1853-2013

O'Neill, B. C., Tebaldi, C., van Vuuren, D. P., Eyring, V., Friedlingstein, P., Hurtt, G., et al. (2016). The scenario model intercomparison project (ScenarioMIP) for CMIP6. *Geoscientific Model Development*, *9*(9), 3461–3482. https://doi.org/10.5194/gmd-9-3461-2016

O'Rourke, P. R., Smith, S. J., Mott, A., Ahsan, H., McDuffie, E. E., Crippa, M., et al. (2021). CEDS v_2021_04_21 release emission data [Dataset]. *Zenodo*. https://doi.org/10.5281/zenodo.4741285

Partanen, A. I., Laakso, A., Schmidt, A., Kokkola, H., Kuokkanen, T., Pietikäinen, J.-P., et al. (2013). Climate and air quality trade-offs in altering ship fuel sulfur content. *Atmospheric Chemistry and Physics*, *13*(23), 12059–12071. https://doi.org/10.5194/acp-13-12059-2013

Peters, K., Stier, P., Quaas, J., & Graßl, H. (2013). Corrigendum to "aerosol indirect effects from shipping emissions: Sensitivity studies with the global aerosol-climate model ECHAM-HAM". *Atmospheric Chemistry and Physics*, *13*(13), 6429–6430. https://doi.org/10.5194/acp-13-6429-2013

Pincus, R., & Baker, M. B. (1994). Effect of precipitation on the albedo susceptibility of clouds in the marine boundary layer. *Nature*, *372*(6503), 250–252. https://doi.org/10.1038/372250a0

Pincus, R., Forster, P. M., & Stevens, B. (2016). The Radiative Forcing Model Intercomparison Project (RFMIP): Experimental protocol for CMIP6. *Geoscientific Model Development*, *9*(9), 3447–3460. https://doi.org/10.5194/gmd-9-3447-2016

Possner, A., Zubler, E., Lohmann, U., & Schär, C. (2016). The resolution dependence of cloud effects and ship-induced aerosol-cloud interactions in marine stratocumulus. *Journal of Geophysical Research: Atmospheres*, *121*(9), 4810–4829. https://doi.org/10.1002/2015JD024685

Quaas, J., Jia, H., Smith, C., Albright, A. L., Aas, W., Bellouin, N., et al. (2022). Robust evidence for reversal of the trend in aerosol effective climate forcing. *Atmospheric Chemistry and Physics*, *22*(18), 12221–12239. https://doi.org/10.5194/acp-22-12221-2022

Quaglia, I., & Visioni, D. (2024). *Modeling 2020 regulatory changes in international shipping emissions helps explain 2023 anomalous warming* (Vol. 2024, pp. 1–19). EGUsphere.

Righi, M., Klinger, C., Eyring, V., Hendricks, J., Lauer, A., & Petzold, A. (2011). Climate impact of biofuels in shipping: Global model studies of the aerosol indirect effect. *Environmental Science & Technology*, *45*(8), 3519–3525. https://doi.org/10.1021/es1036157

Schmidt, G. (2024). Climate models can't explain 2023's huge heat anomaly — We could be in uncharted territory. *Nature*, *627*(467), 467. https://doi.org/10.1038/d41586-024-00816-z

Schoeberl, M. R., Wang, Y., Ueyama, R., Dessler, A., Taha, G., & Yu, W. (2023). The estimated climate impact of the Hunga Tonga-Hunga Ha'apai eruption plume. *Geophysical Research Letters*, *50*(18), e2023GL104634. https://doi.org/10.1029/2023GL104634

Schreier, M., Mannstein, H., Eyring, V., & Bovensmann, H. (2007). Global ship track distribution and radiative forcing from 1 year of AATSR data. *Geophysical Research Letters*, *34*(17). https://doi.org/10.1029/2007gl030664

Sellar, A. A., Jones, C. G., Mulcahy, J. P., Tang, Y., Yool, A., Wiltshire, A., et al. (2019). UKESM1: Description and evaluation of the UK Earth system model. *Journal of Advances in Modeling Earth Systems*, *11*(12), 4513–4558. https://doi.org/10.1029/2019MS001739

Sellitto, P., Podglajen, A., Belhadji, R., Boichu, M., Carboni, E., Cuesta, J., et al. (2022). The unexpected radiative impact of the Hunga Tonga eruption of 15th January 2022. *Communications Earth & Environment*, *3*(1), 1–10. https://doi.org/10.1038/s43247-022-00618-z

Skeie, R. B., Byrom, R., Hodnebrog, Ø., Jouan, C., & Myhre, G. (2024). Multi-model effective radiative forcing of the 2020 sulphur cap for shipping. *EGUsphere*, 1–14. https://doi.org/10.5194/egusphere-2024-1394

Small, J. D., Chuang, P. Y., Feingold, G., & Jiang, H. (2009). Can aerosol decrease cloud lifetime? *Geophysical Research Letters*, *36*(16). https://doi.org/10.1029/2009GL038888

Smith, T. W. P., Jalkanen, J. P., Anderson, B. A., Corbett, J. J., Faber, J., Hanayama, S., et al. (2015). Third IMO GHG study 2014 executive summary and final report. (Tech. Rep.). *International Maritime Organization*.

Sofiev, M., Winebrake, J. J., Johansson, L., Carr, E. W., Prank, M., Soares, J., et al. (2018). Cleaner fuels for ships provide public health benefits with climate tradeoffs. *Nature Communications*, *9*(406), 406. https://doi.org/10.1038/s41467-017-02774-9

Solakivi, T., Laari, S., Kiiski, T., Töyli, J., & Ojala, L. (2019). How shipowners have adapted to sulphur regulations – Evidence from Finnish seaborne trade. *Case Studies on Transport Policy*, *7*(2), 338–345. https://doi.org/10.1016/j.cstp.2019.03.010

Twomey, S. (1974). Pollution and the planetary albedo. *Atmospheric Environment*, *8*(12), 1251–1256. https://doi.org/10.1016/0004-6981(74)90004-3

Twomey, S. (1977). The influence of pollution on the shortwave albedo of clouds. *Journal of the Atmospheric Sciences*, *34*(7), 1149–1152. https://doi.org/10.1175/1520-0469(1977)034⟨1149:TIOPOT⟩2.0.CO;2

Watson-Parris, D., Christensen, M. W., Laurenson, A., Clewley, D., Gryspeerdt, E., & Stier, P. (2022). Shipping regulations lead to large reduction in cloud perturbations. *Proceedings of the National Academy of Sciences of the United States of America*, (Vol. 119(41)). https://doi.org/10.1073/pnas.2206885119

West, R. E. L., Stier, P., Jones, A., Johnson, C. E., Mann, G. W., Bellouin, N., et al. (2014). The importance of vertical velocity variability for estimates of the indirect aerosol effects. *Atmospheric Chemistry and Physics*, *14*(12), 6369–6393. https://doi.org/10.5194/acp-14-6369-2014

Wilks, D. S. (2006). On "field significance" and the false discovery rate. *Journal of Applied Meteorology and Climatology*, *45*(9), 1181–1189. https://doi.org/10.1175/JAM2404.1

Wilks, D. S. (2016). "The stippling shows statistically significant grid points": How research results are routinely overstated and overinterpreted, and what to do about it. *Bulletin of the American Meteorological Society*, *97*(12), 2263–2273. https://doi.org/10.1175/BAMS-D-15-00267.1

Williams, K. D., Copsey, D., Blockley, E. W., Bodas-Salcedo, A., Calvert, D., Comer, R., et al. (2018). The Met Office global coupled model 3.0 and 3.1 (GC3.0 and GC3.1) configurations. *Journal of Advances in Modeling Earth Systems*, *10*(2), 357–380. https://doi.org/10.1002/2017MS001115

Wilson, D. R., & Ballard, S. P. (1999). A microphysically based precipitation scheme for the UK meteorological office unified model. *Quarterly Journal of the Royal Meteorological Society*, *125*(557), 1607–1636. https://doi.org/10.1002/qj.49712555707

Wilson, D. R., Bushell, A. C., Kerr-Munslow, A. M., Price, J. D., & Morcrette, C. J. (2008). PC2: A prognostic cloud fraction and condensation scheme. I: Scheme description. *Quarterly Journal of the Royal Meteorological Society*, *134*(637), 2093–2107. https://doi.org/10.1002/qj.333

Woodward, S. (2001). Modeling the atmospheric life cycle and radiative impact of mineral dust in the Hadley Centre climate model. *Journal of Geophysical Research*, *106*(D16), 18155–18166. https://doi.org/10.1029/2000JD900795

Yool, A., Popova, E. E., & Anderson, T. R. (2013). MEDUSA-2.0: An intermediate complexity biogeochemical model of the marine carbon cycle for climate change and ocean acidification studies. *Geoscientific Model Development*, *6*(5), 1767–1811. https://doi.org/10.5194/gmd-6-1767-2013

Yoshioka, M., Grosvenor, D. P., Booth, B. B. B., Morice, C. P., & Carslaw, K. S. (2024). Warming effects of reduced sulfur emissions from shipping. *EGUsphere*, *2024*, 1–19. https://doi.org/10.5194/egusphere-2024-1428

Yuan, T., Song, H., Oreopoulos, L., Wood, R., Bian, H., Breen, K., et al. (2023). Substantial radiative warming by an inadvertent geoengineering experiment from 2020 fuel regulations. *Research Square*. https://doi.org/10.21203/rs.3.rs-3490826/v1

Yuan, T., Song, H., Oreopoulos, L., Wood, R., Bian, H., Breen, K., et al. (2024). Abrupt reduction in shipping emission as an inadvertent geoengineering termination shock produces substantial radiative warming. *Communications Earth & Environment*, *5*(1), 1–8. https://doi.org/10.1038/s43247-024-01442-3

Yuan, T., Song, H., Wood, R., Wang, C., Oreopoulos, L., Platnick, S. E., et al. (2022). Global reduction in ship-tracks from sulfur regulations for shipping fuel. *Science Advances*, *8*(29), eabn7988. https://doi.org/10.1126/sciadv.abn7988

References From the Supporting Information

Jones, A., & Haywood, J. M. (2012). Sea-spray geoengineering in the hadgem2-es earth-system model: Radiative impact and climate response. *Atmospheric Chemistry and Physics*, *12* (22), 10887–10898. https://doi.org/10.5194/acp-12-10887-2012

Mahfouz, N. G. A., Hill, S. A., Guo, H., & Ming, Y. (2023). The radiative and cloud responses to sea salt aerosol engineering in GFDL models. *Geophysical Research Letters*, *50* (2), e2022GL102340. https://doi.org/10.1029/2022GL102340